J Mater Sci (2011) 46:2938–2946
DOI 10.1007/s10853-010-5169-x

Structure and properties of novel electrospun tussah silk fibroin/poly(lactic acid) composite nanofibers

Jianxin He · Yongrui Qin · Shizhong Cui · Yaying Gao · Shanyuan Wang

Received: 9 July 2010 / Accepted: 7 December 2010 / Published online: 17 December 2010

Abstract The tussah silk fibroin (TSF)/poly(lactic acid) (PLA) composite nanofibers with different composition ratios were prepared by electrospinning with 1,1,1,3,3,3-Hexafluoro-2-propanol as the solvent. The morphology and secondary structure of the fibers were characterized by Scanning electronic microscope, Fourier transform infrared (FTIR), and X-ray diffraction (XRD). The thermal and mechanical tests were also performed. The spinnability of TSF solution was improved significantly through adding 10% PLA, and the average diameter of the fibers decreased from 583 nm to 178 nm with an obvious improvement in fiber diameter uniformity. In addition, the mechanical properties of electrospun nanofibers increased evidently after blending 10% PLA, whereas the thermal properties kept stable. FTIR and XRD analysis indicated the addition of 5% PLA could induce a conformation transformation of TSF from random coil and α-helix to β-sheet, however, when PLA content was more than 10%, the β-sheet structure of TSF in composite nanofibers decreased, and the phase separation of two compositions occurred. Therefore, when PLA content exceeded 15%, the average diameters of TSF/PLA composite nanofibers increased and appeared to be polarized, moreover, the mechanical properties of the fibers decreased with the increase of PLA content, and the fibers displayed the mechanical behavior of PLA component more.

J. He (✉) · Y. Gao · S. Wang
College of Textiles, Donghua University,
Shanghai 201620, People's Republic of China
e-mail: hejianxin771117@163.com

J. He · Y. Qin · S. Cui
Henan Key Laboratory of Textile Materials, Zhongyuan
University of Technology, Zhengzhou 450007,
People's Republic of China

Introduction

The goal of tissue engineering is to construct the tissue engineering scaffold material, which can mimic the fibrillar structure of the extracellular matrix (ECM), to provide a essential guidance for cell organization, survival, and function and then to develop feasible substitutes to aid in the clinical treatment. Electrospinning technique is a simple and effective method to produce polymer nanofibers with diameter in the range from several micrometers down to tens of nanometers. In electrospinning, a high voltage is applied to create electrically charged jets of a polymer solution. These jets were dried to form nanofibers, which are collected on a target as non-woven mat [1]. Three-dimensional nanofibrous scaffolds prepared by electrospinning technique are regarded as ideal material for tissue engineering because they can not only mimic the nanosized dimension of natural ECM but can also form a defined architecture to guide cell growth and development as needed [2].

Silk fibroin (SF) is the protein that forms filaments of silkworm silk and give silk high mechanical strength, elasticity, and softness. In addition to the outstanding mechanical properties, SF displays good biocompatibility, biodegradability, non-cytotoxicity, and minimal inflammatory reaction [3]. Many studies have indicated that electrospun SF nanofiber mats were very effective on the adhesion and proliferation of cells such as fibroblast, osteoblast, and human keratinocyte [4, 5]. SF has been electrospun with different solvents [6, 7] or by blending with other polymer such as chitosan [8], chitin [9], gelatin [10], etc.

Nevertheless, these electrospun SF nanofibers are based on *B. mori* silk. Tussah silk is one of the wild silks, and its chemical structure, molecular conformation, and physical

properties have been extensively studied. In contrast to *B. mori* silk, its amino acid composition is characterized by more Ala, Asp, and Arg contents and less Gly [11]. Moreover, it is well known that the presence of the tripeptide sequence Arg–Gly–Asp (RGD) may act as a biological recognition signal, promoting cell adhesion and consequently, make tussah silk fibroin (TSF) suitable for biomedical application [12, 13]. However, because tussah silk contains abundant $-(Ala)_n-$ sequence in crystalline region, the dissolution of tussah silk fibers is difficult [14]. In our previous study, TSF was electrospun with HFIP as the solvent, but TSF showed a poor spinnability and the electrospun fibers presented a belt-like morphology with a wide diameter distribution.

Poly(lactic acid) (PLA) is biocompatible and undergoes scission in the body to lactic acids. These characteristic make PLA suitable for many biomedical applications. However, PLA is strongly lipophilic and still lacks mechanical integrity [15], thus the modification of PLA has also attracted significant attention.

In this article, electrospun TSF/PLA composite nanofibers were prepared in order to obtain a better nanofibrous scaffold for tissue engineering by combining their respective advantages. The effect of PLA content on the morphology, secondary structure, thermal, and mechanical properties of electrospun nanofibers was investigated, and the results indicated that TSF/PLA composite nanofibers with 10% PLA exhibited a uniform rod-like morphology with narrower diameter distribution and excellent mechanical properties.

Experimental

Materials

Antheraea pernyi cocoon came from Henan province, China. 1,1,1,3,3,3-Hexafluoro-2-propanol (HFIP) and poly (lactic acid) (MW 232 kDa) was supplied by Shanghai Chemical reagent Co. Ltd., China. All chemical reagents are analytical reagent.

Preparation of TSF/PLA blend solution

Antheraea pernyi cocoons were degummed using 0.5% Na_2CO_3 solution at 98 °C for three times. Degummed tussah fibers were dissolved in 9 M aqueous lithium thiocyanate solution at a liquor ratio of 10:1 by stirring at 55 °C for 1 h. Then the TSF aqueous solution was filtered to remove undissolved part, and then dialyzed for 3 days in distilled water. The TSF solution was lyophilized to obtain the regenerated TSF sponge. The TSF sponge and PLA were dissolved in HFIP at different weight ratios (100/0, 95/5, 90/10, 85/15, 70/30, 60/40, 0/100, w/w) to obtain a spinning solution of 8 wt% for electrospinning.

Preparation of electrospun TSF/PLA composite nanofibers

The electrospinning apparatus was composed of a high voltage power supply, a syringe pump, a syringe, and needle (0.9 mm OD × 0.5 mm ID) and a rectangular (20 × 10 cm) aluminum foil collecting plate. The schematic diagram of the electrospinning process is shown in Fig. 1. The TSF/PLA blend solution was placed into a 10 ml syringe with a stainless needle connected the positive electrode of a high voltage power supplier, and its negative electrode was clipped in the aluminum foil. Under the influence of the electrostatic field, a droplet at the tip of the needle is jet into a conical shape. When the electric field is sufficiently strong, charges built on the surface of the droplet will overcome the surface tension of the droplet to induce many charged jets that are subsequently accelerated toward a collector. Due to the high viscosity of the polymer solution and the presence of chain entanglements, the jet exhibits nonlinear rheologic behavior and therefore forms a liquid thread jet. As the polymer jets progress toward the collector, the external electric field stretches and splays the polymer jets into fibers.

All electrospinning experiments were performed with the same processing condition. The spinning distance between the needle tip and the aluminum foil was 10 cm. The voltage applied to the needle was 12 kV, and the flow rate was 0.3 ml/h controlled by the syringe pump.

Characterization

The samples collected were coated with gold film in order to observe the morphology of electrospun nanofibers. The instrument was a JEOL JSM-5600LV electron microscopic with an accelerating voltage of 15 kV. The fiber diameter distributions are sampled from 100 different locations of fiber-crossing on the SEM micrographs.

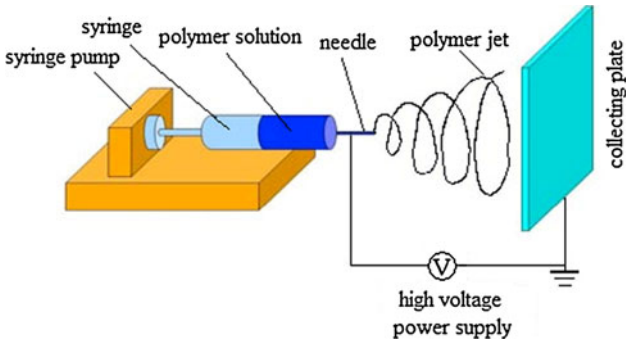

Fig. 1 Schematic diagram of electrospinning process

FTIR spectra of TSF/PLA composite nanofibers were recorded with a Nicolet Nexus 670 FTIR spectrometer, using the KBr disc technique (1 mg powdered nanofiber sample/300 mg KBr). 100 Scans were taken with a resolution of 2 cm^{-1}.

X-ray diffractions of powdered electrospun fibers were record at a scanning speed of 0.02°/s with a Rigaku-D/Max-2550PC diffractometer using Ni-filtered Cu K_α radiation of wavelength 0.1542 nm. The operating voltage and current were 40 kV and 30 mA, respectively.

Thermogravimetric (TG) analysis was carried out on Perkin Elmer TGA thermogravimetric analysis instrument. All the experiments were carried out with the same nitrogen flux. The heating-up speed was 10 °C/min and the degradation temperature was from 25 to 500 °C.

Mechanical property

The stress–strain curve was recorded on an Instron tester (Model 3365) at room temperature under room humidity. The electrospun nonwoven mats with 2 mm width and 30 mm original length were prepared. The thickness of the samples was from 0.15 to 0.30 mm. The gauge length was set to be 15 mm and the rate of the crosshead was 10 mm/min. The reported data of tensile strength and elongation represent the average results of ten tests.

Results and discussion

Fiber morphology

The electrospinning process of pure TSF solution had been first optimized before the electrospinning of TSF/PLA blend solution, and the best spinning conditions were identified as: a concentration of 8%, a voltage of 12 kV and a spinning distance of 10 cm. The electrospinning of pure PLA solution and the TSF/PLA blends with different composition ratios was performed in these conditions. Figure 2 shows the SEM photographs of electrospun pure TSF, pure PLA, and TSF/PLA composite nanofibers obtained in the same spinning conditions.

In contrast to the silk fibroin from *B. mori* silk, TSF showed a poor spinnability in electrospinning. Electrospun TSF nanofibers present a belt-like morphology with a wide diameter distribution (Fig. 2a). However, many literatures have been reported that a rod-like morphology with a uniform fiber structure could be obtained in electrospinning of *B. mori* silk fibroin using HFIP as solvent [16]. In addition, due to the incomplete solvent evaporation and jet split, fibers' adhesion and bifurcation were also observed in the TSF electrospinning. This is mainly because the amino acid sequences in the crystalline regions of *B. mori* silk fibroin and TSF are composed of —$(Gly\text{-}X)_n$— (X is Ala or Trp residues) sequence and —$(Ala)_n$— sequence, respectively [17]. Therefore, the crystalline region in TSF has a more compact molecular structure, which leads to a poor solubility of TSF in HFIP solvent. The serious tangling of TSF molecules in solution will make the drawing and shaping of fibers become difficult in electrospinning.

The product of PLA electrospinning presents a coexistence of continuous fibers and beats (Fig. 2g), but this did not mean the poor spinnability of PLA, and the cause was the lower viscosity of PLA solution at a concentration of 8%. When PLA concentration was up to 10%, the electrospun nanofibers with a uniform and regular morphology could be obtained (no shown).

PLA content has a great effect on the morphology of composite nanofibers. Figure 3 shows the diameter distribution of electrospun nanofibers, and the effect of PLA content on the fiber diameters is shown in Fig. 4. When adding 5% PLA, the electrospun composite nanofibers looked slightly uniform (Fig. 2b), and the average diameter reduced from 583 nm to 426 nm. But the most significant change occurred in the PLA content of 10% (Fig. 2c), here the average fiber diameter decreased to 178 nm and its distribution was narrowest (Fig. 4). The addition of PLA can lead to the decrease of the viscosity of TSF solution. In addition, a small amount of PLA in blend solution can induce a structure change of TSF from random coil to order β-sheet (see latter). Thus these are favorable for extending molecular chains through electrostatic force to form thin and uniform nanofibers. When the PLA content reached 15%, TSF/PLA composite nanofibers still had a regular morphology (Fig. 2d), but the average diameter increased and the diameter distribution became broader. As the PLA content in blend was higher than 15%, a polarization in fiber diameters could be observed as shown in (Fig. 2e, f), and the electrospun fiber mats in these cases were friable, demonstrating an obvious phase separation appeared in these electrospun composite fibers.

FTIR spectra

FTIR is a powerful and common tool for the protein conformation analysis, and therefore is widely used the study of silk fibroin. FTIR spectra of TSF/PLA composite nanofibers are shown in Fig. 5. Electrospun pure TSF nanofibers show three absorption at 1650 cm^{-1} (amide I), 1541 cm^{-1} (amide II), and 1261 cm^{-1} (amide III), which can be attributed to α-helix or random coil conformation, whereas the shoulder peak at 1517 cm^{-1} (amide II) and the peak at 1230 cm^{-1} (amide III) are attributed to β-sheet conformation [18]. It means that α-helix and β-sheet conformations coexist in the pure TSF nanofibers, and α-helix conformation is predominant.

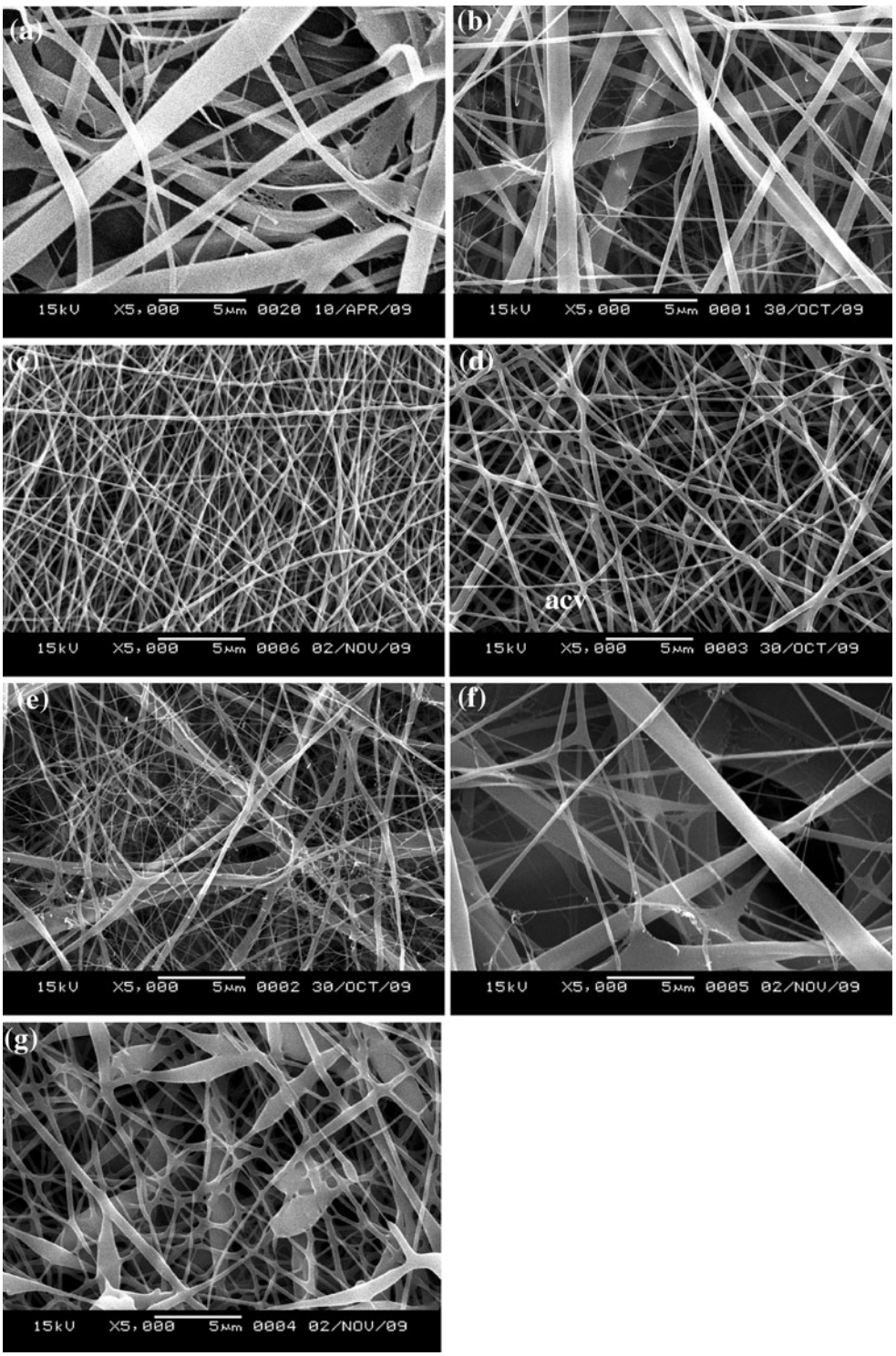

Fig. 2 SEM micrographs of **a** pure TSF nanofibers, TSF/PLA composite nanofibers containing **b** 5%, **c** 10%, **d** 15%, **e** 30%, and **f** 40% PLA, and **g** pure PLA nanofibers

TSF/PLA composite nanofibers show absorption bands characteristic of both TSF and PLA components overlapping. The spectrum of pure PLA nanofibers is characterized by absorption peaks at 1757 cm^{-1} (the stretching of C = O), 1452 cm^{-1} (the blending of CH_3), and 1385 cm^{-1} (the symmetric deformation of CH_3). In addition, there have the absorption peaks at 1267, 1184, and 1090 cm^{-1}, assigned to the stretching of C–O–C in PLA. These peaks

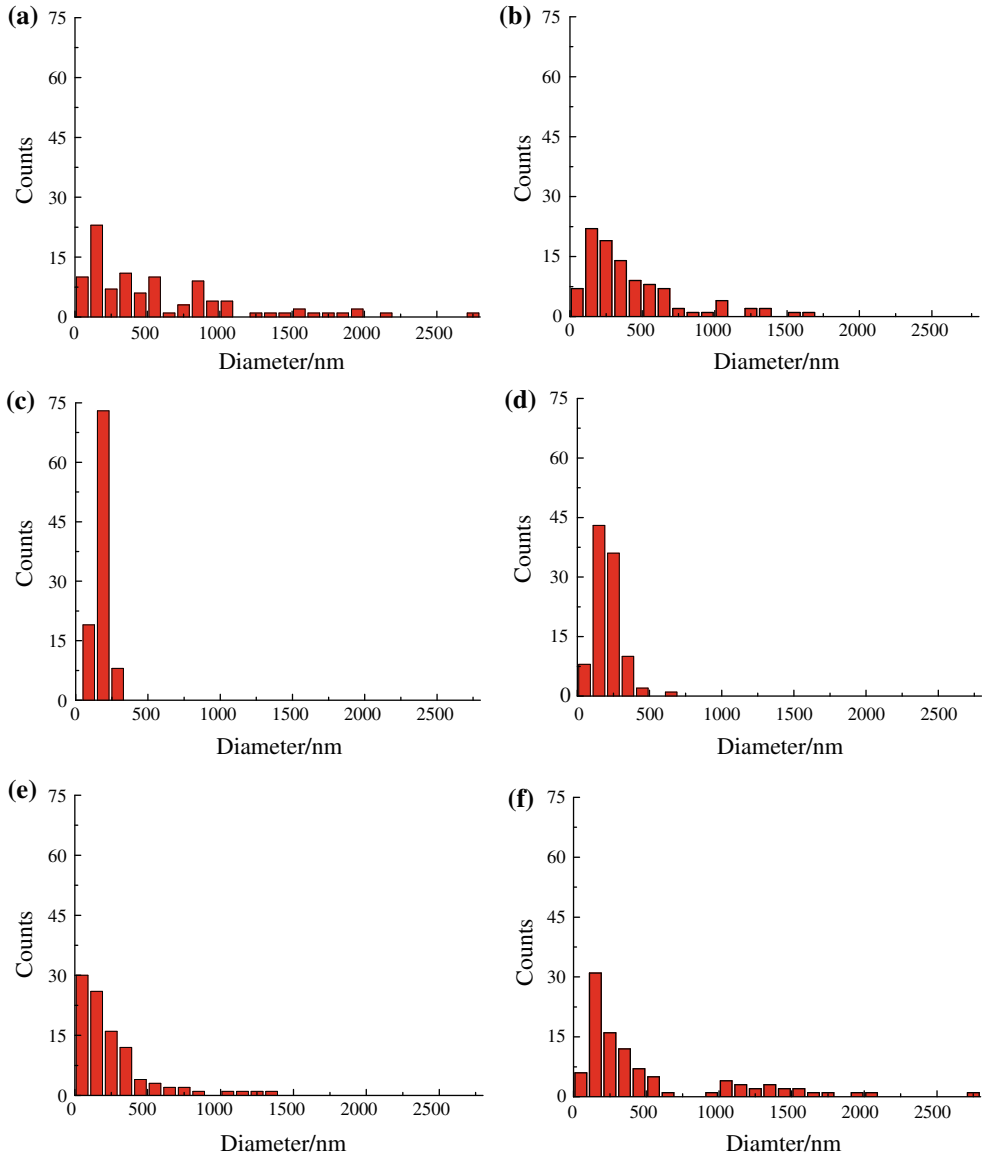

Fig. 3 Diameter distribution graphs of **a** electrospun pure TSF nanofiber mats and electrospun TSF/PLA composite nanofiber mats with **b** 5%, **c** 10%, **d** 15%, **e** 30%, and **f** 40% PLA

in composite nanofibers enhanced with the increase of PLA content. Because the characteristic peaks of TSF in amide I and II regions did not overlapped with the absorption peaks of PLA, the change of the secondary structure of TSF in composite nanofibers can be judged by analyzing the peaks in amide I and II region.

In amide I region, the sharp peak of TSF nanofibers at 1650 cm^{-1} attributed to α-helix conformation changed into a broad peak after adding 5% PLA, however, when PLA content increased to 10%, this peak enhanced again. In amide II region, the TSF nanofibers exhibited a doublet at 1541 and 1517 cm^{-1}, assigned to α-helix/random coil and β-sheet, respectively. The relative intensity of the peak at 1541 cm^{-1} decreased after adding 5%PLA, while this peak increased further when PLA content exceeded 5%. These modifications seem to indicate a conformation transition of TSF from random coil/α-helix to β-sheet after blending 5% PLA in composite nanofibers. However, when PLA content was up to 10%, the β-sheet content of TSF decreased in electrospun TSF/PLA composite nanofibers.

X-ray diffraction analysis

Figure 6 shows the diffraction patterns of TSF/PLA composite nanofibers. Electrospun pure PLA fibers with irregular morphology prepared in this article presented a weak crystalline structure with weak diffraction peaks at 2θ of 10.4°, 14.6°, 16.6°, and 20.0° (Fig. 6f). X-ray diffraction

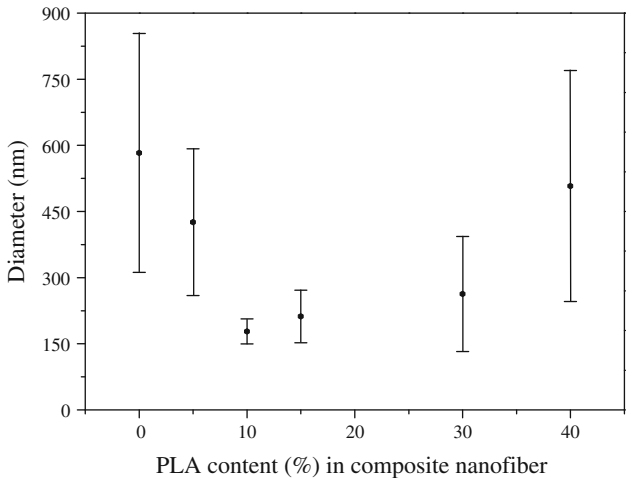

Fig. 4 Diameter and its distribution of electrospun TSF/PLA composite nanofibers

curve of pure TSF nanofibers consisted of two apparent peaks, a sharp peak at 2θ of 10.4° and a broad peak at about 21.5° (Fig. 6a). The former is the characteristic peak of α-helix crystal, and the latter should be the superposition of some minor peaks, including the peak at 2θ of 19.2° attributed to β-sheet crystal and the peaks at 21.5° and 23.0° attributed to α-helix crystals [19, 20]. In addition, a shoulder peak at 12.2° should be attributed to α-helix crystal in diffraction curve of TSF nanofiber [21]. Therefore, X-ray diffraction pattern also proved that α-helix and β-sheet structure coexisted in pure TSF nanofibers, and α-helix structure showed a higher content.

Significant changes could be observed in X-ray diffraction pattern of TSF nanofibers after adding 5% PLA. For the broad peak of TSF nanofibers at about 21.5°, the peak position at maximum diffraction intensity shifted from 21.5° to the 19.2°, moreover, the peak at 12.2° assigned to α-helix conformation of TSF disappeared, while a peak at 31.0° appeared, which was assigned to the β-sheet conformation of TSF. These also conform that adding 5% PLA induced a conformation change of TSF from α-helix to β-sheet, which is consistent to the result of FTIR analysis.

When PLA content reached 10% or more, electrospun TSF/PLA nanofibers showed another X-ray diffraction pattern, presenting a peak superposition of pure TSF and PLA nanofibers. In the case of composite nanofibers with 10% PLA, the fibers exhibited a shoulder peak at 16.6° attributed to PLA in addition to the peak at 10.4° corresponding to α-helix crystal of TSF. When PLA content in composite nanofibers was more than 10%, three major peaks of PLA at 14.6°, 16.6°, and 20.0° could be observed without exception. This suggests that when PLA content increased to 10%, phase separation began to appear in

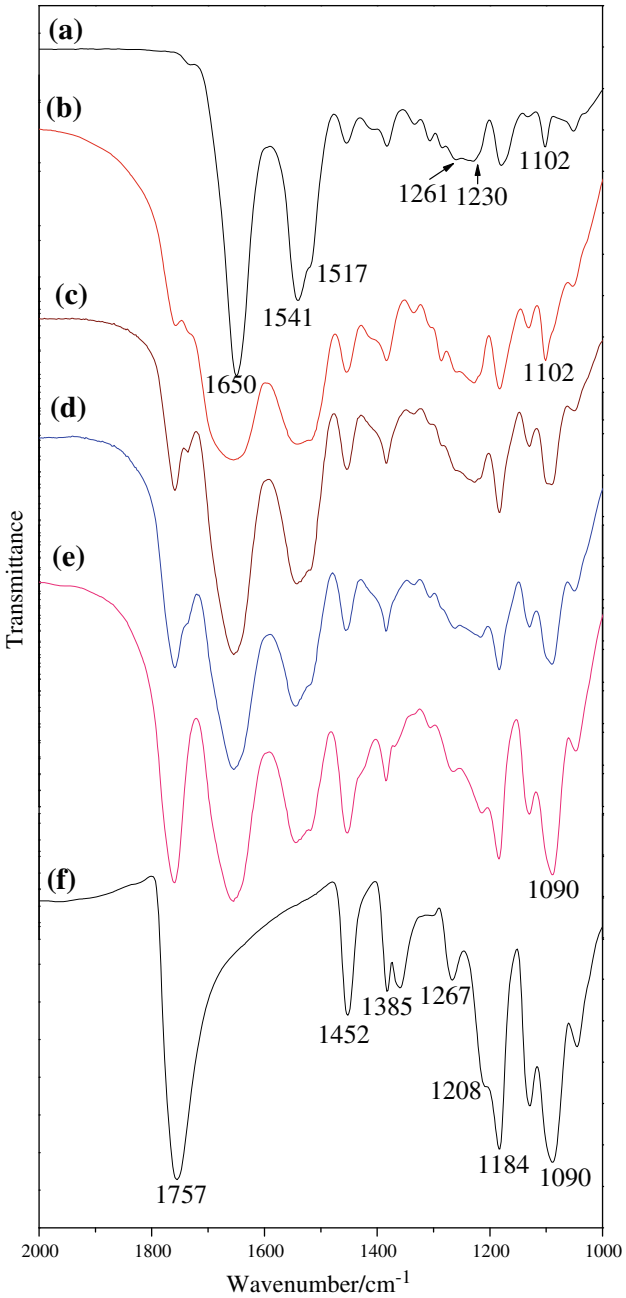

Fig. 5 FTIR spectra of (*a*) pure TSF nanofibers, TSF/PLA composite nanofibers containing (*b*) 5%, (*c*) 10%, (*d*) 15%, and (*e*) 40% PLA, and (*f*) pure PLA nanofiber

electrospun TSF/PLA composite nanofibers, and with the increase of PLA content, phase separation became more obvious. Thus reflected in the morphology of nanofibers, when PLA content in composite nanofibers was more than 15%, the polarization of fiber diameter could be found. However, the composite nanofibers containing 10% PLA showed the most uniform and regular morphology with the narrowest diameter distribution, which should be the result

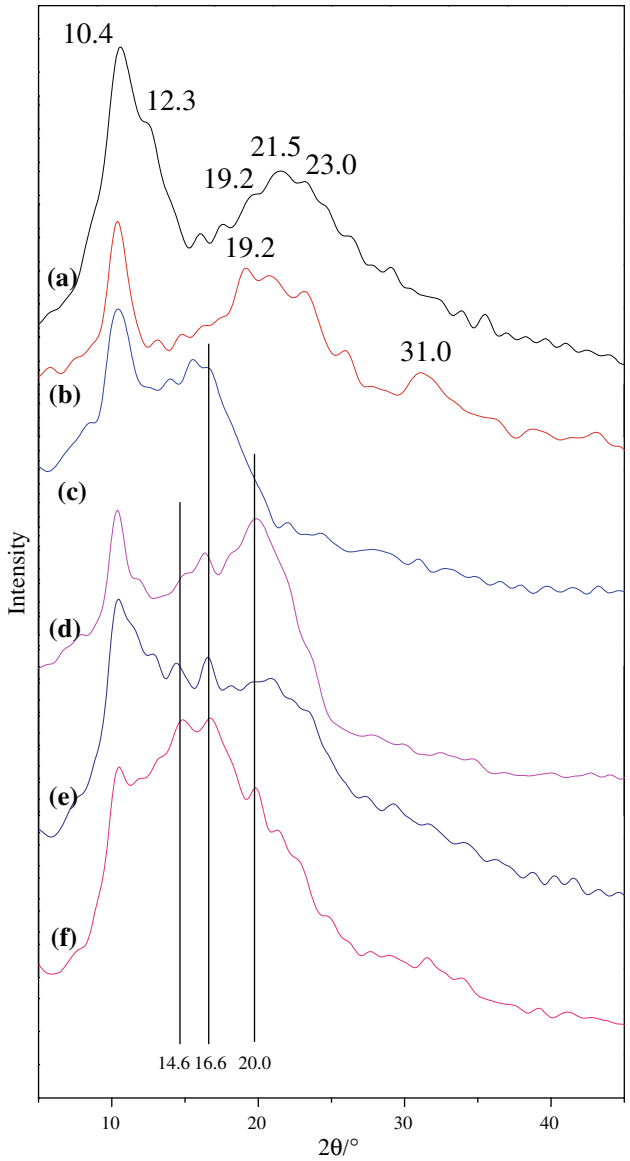

Fig. 6 X-ray diffraction patterns of (*a*) pure TSF nanofibers, TSF/PLA composite nanofibers containing (*b*) 5%, (*c*) 10%, (*d*) 15% ,and (*e*) 40% PLA, and (*f*) pure PLA nanofiber

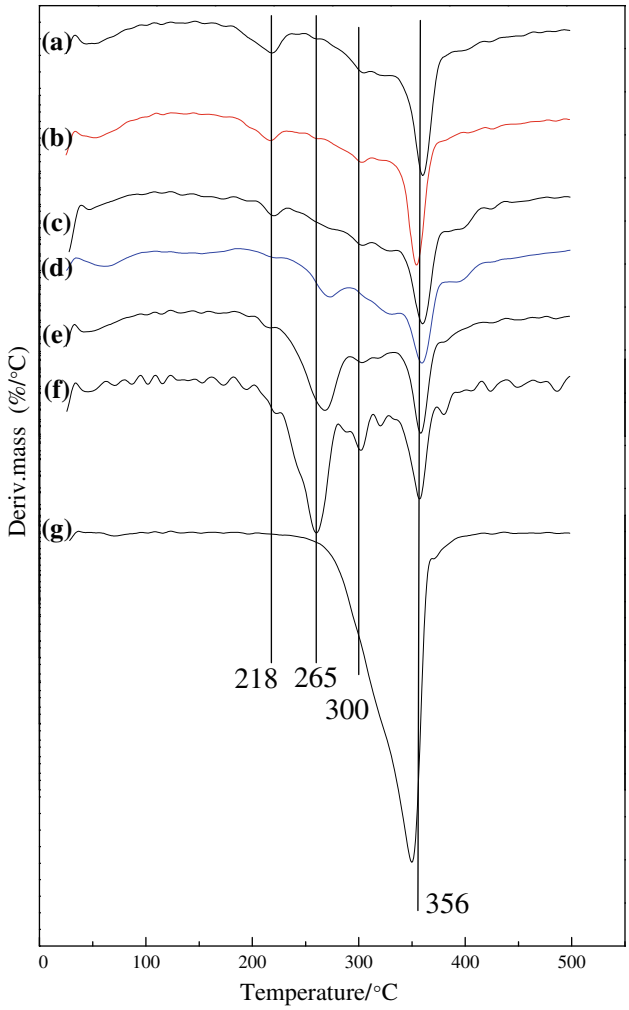

Fig. 7 DTG curves of (*a*) pure TSF nanofibers, TSF/PLA composite nanofibers containing (*b*) 5%, (*c*) 10%, (*d*) 15%, (*e*) 30%, and (*f*) 40% PLA, and (*g*) pure PLA nanofibers

from the synergistic effect of the decrease in spinning solution viscosity and the conformational change of TSF.

Thermogravimetric analysis

The DTG curves of electrospun TSF/PLA composite nanofibers are shown in Fig. 7. Obviously, at the first peak between 40 and 100 °C in these DTG curves, the weight loss was due to water vaporization. Pure TSF nanofiber showed three major decomposition peaks at 218, 265, and 359 °C, while pure PLA nanofibers exhibited a decomposition peak at 260–400 °C with maximum weight loss at 349 °C. Adding 5–10% PLA into TSF solution did not affect the thermal decomposition of nanofibers, but the initial decomposition peak of TSF at 218 °C reduced, indicating a decrease of weight loss. This can be explained by the β-sheet crystallization of TSF induced by PLA [22].

When PLA content arrived at 15% in composite nanofibers, a new decomposition peak appeared at around 270 °C, which increased at peak intensity but shifted to lower temperature with the increase of PLA content. As PLA content increased to 40%, electrospun TSF/PLA composite nanofibers showed a more complex decomposition behavior with the other two minor peaks appearing between the peaks at 270 and 359 °C. However, in these blend ratios the composite nanofibers did not exhibited the decomposition peak of pure PLA at 349 °C, which should not overlapped with the decomposition peak of TSF at 359 °C because the peak at 359 °C reduced with the

increase of PLA content. Thus, the decomposition peak of composite nanofibers at around 270 °C in the case of 15% PLA or more, and the two minor peaks between the peaks at 270 and 359 °C are likely attributed to the decomposition of PLA in composite nanofibers. Because TSF contains more polar amino acids than *B. mori* silk [23], the acidic and basic groups in these amino acids can catalyze the decomposition of PLA, leading to the decomposition peak of PLA at a lower temperature and showing multi-stage decomposition behavior.

Mechanical properties

The stress–strain curves of TSF/PLA composite nanofiber mats are shown in Fig. 8. The composite nanofiber mats with various PLA content displays a different mechanical behavior. In contrast with pure TSF nanofiber mats, the composite nanofiber mats with 10% PLA showed a remarkable increase in mechanical properties with a breaking stress from 1.158 to 2.727 MPa and a breaking strain from 4.05 to 4.39% (Table 1). The improvement in mechanical properties of the nanofiber mat after blending 10% PLA may be attributed to an increase in the β-sheet content of TSF. However, as the PLA content increased to 30%, the breaking stress of TSF/PLA composite nanofiber mats decreased whereas the breaking strain increased obviously. Because the apparent phase separation occurred in the composite nanofibers with 30 and 40% PLA, these nanofiber mats showed a similar mechanical behavior to PLA fibers, which exhibit a lower breaking stress whereas a greater stress [24]. In addition, the mechanical properties of nanofiber mats depended in this case on surface tensions of the nanofibers [25, 26], more hydrophobic PLA made the surface tensions of the TSF/PLA composite nanofibers decrease. It is noteworthy that the breaking stress of nanofiber mats showed little changes between 0 and 30% PLA, however, there was a sudden increase of breaking stress when going to 40% PLA. This means a large decrease of the brittleness of the composite nanofiber mats between 30 and 40% PLA more likely due to the deteriorative phase separation [27, 28].

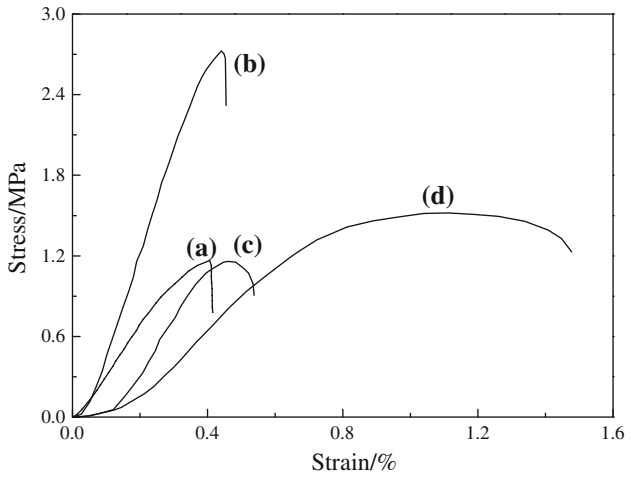

Fig. 8 Stress-strain curves of (*a*) electrospun pure TSF nanofiber mats and electrospun TSF/PLA composite nanofiber mats with (*b*) 10%, (*c*) 30%, and (*d*) 40% PLA

Table 1 Mechanical properties of electrospun TSF/PLA nanofiber mats

PLA content (%)	Breaking stress		Breaking strain (%)	
	Mean(MPa)	CV	Mean (%)	CV
0	1.158	9.65	4.05	14.24
5	1.958	8.15	3.98	11.52
10	2.727	6.82	4.39	10.89
15	1.862	8.17	4.50	13.23
30	1.158	9.25	4.63	15.18
40	1.519	9.87	10.95	15.96

References

1. Patra SN, Easteal AJ, Bhattacharyya D (2009) J Mater Sci 44:647. doi:10.1007/s10853-008-3050-y
2. Li WJ, Laurencin CT, Caterson EJ, Tuan RS, Ko FK (2002) J Biomed Mater Res 60:613
3. Tretinnikov ON, Tamada Y (2001) Langmuir 17:7406
4. Min BM, Lee G, Kim SH, Nam YS, Lee TS, Park WH (2004) Biomaterials 25:1289
5. Zhang F, Zuo BQ, Bai L (2009) J Mater Sci 44:5682. doi: 10.1007/s10853-009-3800-5
6. Ohgo K, Zhao C, Kobayashi M, Asakura T (2003) Polymer 44:841
7. Chen C, Cao CB, Ma X, Tang Y, Zhu H (2006) Polymer 47:6322
8. Park WH, Jeong L, Yoo DI, Hudson S (2004) Polymer 45:7151
9. Park KE, Jung SY, Lee SJ, Min BM, Park WH (2006) Int J Biol Macromol 38:165
10. Yin G, Zhang Y, Bao W, Wu J, Shi D, Dong Z, Fu W (2009) J Appl Polym Sci 111:1471
11. Nakazawa Y, Asakura T (2002) Macromolecules 35:2393
12. Pierschbacher MD, Ruoslahti E (1984) Nature 30:309
13. He J, Wang Y, Cui S, Gao Y, Wang S (2010) Iran Polym J 19:625
14. Kweon HY, Park YH (2001) J Appl Polym Sci 82:75
15. Wnek GE, Carr ME, Simpson DG, Bowlin GL (2003) Nano Lett 3:213
16. Zarkoob S, Reneker DH (1998) Polymer 39:244
17. Inoue S, Magoshi J, Tanaka T, Magoshi Y, Becker M (2000) J Polym Sci Part B Polym Phys 38:1436
18. Freddi G, Monti P, Nagura M, Gotoh Y, Tsukada M (1997) J Polym Sci Part B 35:841
19. Kweon HY, Woo SO, Park YH (2000) J Appl Polym Sci 81:2271
20. Kweon HY, Park YH (1999) J Appl Polym Sci 73:2887
21. Li MZ, Tao W, Kuga S, Nishiyama Y (2003) Polym Adv Technol 14:694

22. Kweon HY, Um IC, Park YH (2000) Polymer 41:7361
23. Freddi G, Gotoh Y, Tsutsui T, Tsukada M (1994) J Appl Polym Sci 53:775
24. Inai R, Kotaki M, Ramakrishna S (2005) Nanotechnology 16:208
25. Stamboulis A, Baillie C, Schulz E (1999) Macromol Mater Eng 272:117
26. Kopczynska A, Ehrenstein GW (2007) J Mater Ed 29:325
27. Brostow W, Hagg Lobland HE, Narkis M (2006) J Mater Res 21:2422
28. Brostow W, Hagg Lobland HE (2010) J Mater Sci 45:242. doi:10.1007/s10853-009-3926-5